https://doi.org/10.5194/nhess-2023-18
Preprint. Discussion started: 22 February 2023

Natural Hazards and Earth System Sciences
Discussions

The impact of GNSS Zenith Total Delay data assimilation on the short-term precipitable water vapor and precipitation forecast over Italy using the WRF model

Rosa Claudia Torcasio[1], Alessandra Mascitelli[1], Eugenio Realini[2], Stefano Barindelli[2], Giulio Tagliaferro[3], Silvia Puca[4], Stefano Dietrich[1], Stefano Federico[1]

[1] National Research Council of Italy, Institute of Atmospheric Sciences and Climate (CNR-ISAC), via del Fosso del Cavaliere 100, 00133 Rome, Italy
[2] Geomatics Research & Development srl (GReD), via Cavour 2, 22074 Lomazzo, Italy
[3] BIPM Time Department, Sèvre, France
[4] Civil Protection Department, via Vitorchiano 4, 00189 Rome, Italy

Correspondence to: Stefano Federico (s.federico@isac.cnr.it)

Abstract. The impact of assimilating GNSS-ZTD (Global Navigation Satellite Systems - Zenith Total Delay) on the precipitable water vapor and precipitation forecast over Italy is studied for the month of October 2019, characterized by several moderate to intense precipitation events. The WRF (Weather Research and Forecasting) model 4.1.3 is used with its 3DVar data assimilation system to assimilate ZTD observations from 388 GNSS receivers distributed over the country. The dataset was built collecting data from all the major national and regional GNSS permanent networks, achieving dense coverage over the whole area.

Results show that WRF underestimates the atmospheric water vapor content for the period, and GNSS-ZTD data assimilation improves this underestimation.

The water vapor forecast is verified for the forecast hours 1-6h after the last data assimilation time, while the precipitation forecast is verified in the phases 0-3h and 3-6h after the last data assimilation time. More than 3000 rain gauges spread over Italy were used to verify the precipitation forecast.

The application of GNSS-ZTD data assimilation to a case study showed an improvement of the precipitation forecast in different ways, the main drawback being the prediction of false alarms.

Considering the study over the whole period, GNSS-ZTD data assimilation had a positive impact on the precipitable water vapor and rainfall forecast, with an improvement of the performance up to 6 hours, and with statistically significant results for moderate to intense rainfall thresholds (25-30 mm/3h).

https://doi.org/10.5194/nhess-2023-18
Preprint. Discussion started: 22 February 2023

Natural Hazards and Earth System Sciences
Discussions

1 Introduction

The Mediterranean area is often struck by severe weather and deep convective events because of the presence of the warm sea, the complex orography of the area, and the specific synoptic scale environment. This scenario is worsened by the climate change, which is affecting many weather and climate extremes, and the frequency and intensity of heavy precipitation events have increased in most of the world (Masson-DelMotte et al., 2021).

Over the past years, the use of Numerical Weather Prediction (NWP) models, along with an increasing availability of computing power, led to an improvement of the forecast accuracy. However, NWPs have well-known difficulties in representing the physical processes at small spatial and temporal scales, which are involved in convective or severe weather events (Stensrud et al., 2009).

One of the common problems of NWP-based nowcasting and short-term forecasting is the spin up time, because the model needs a few hours to balance the inconsistencies between the initial and boundary conditions to properly reproduce the small-scale dynamic (Lagasio et al., 2019). Data assimilation of local observations in NWP has been reported as a key factor to reduce this issue and to improve the prediction of high impact weather events (Federico et al., 2021). Among local observations, water vapor plays a key role for its importance in humid and energetic exchanges in the atmosphere. Therefore, a good knowledge of water vapor distribution in space and time is a fundamental requirement for improving NWP forecasts of convective and severe weather events.

Global Navigation Satellite System (GNSS – collective term used to address all global and regional satellite navigation systems, including GPS, Galileo, GLONASS and BeiDou) routine observations processing for geodetic and geophysical purposes can provide estimates of the tropospheric delays (generally ZTD-Zenith Total Delay), directly connected to the water vapor content in the atmosphere, which can be very useful to improve the NWP forecast. Relevant, albeit non exhaustive, experiences are shortly summarized hereafter:

- Vedel and Huang (2004) assimilated GNSS-ZTD into the HIgh Resolution Limited Area Model using 3DVar and found improvements for the forecast of geopotential height and high precipitations.
- Poli et al. (2007), assimilated the GNSS-ZTD using 4DVar and the ARPEGE (Action de Researche Petite Echelle Grande Echelle) global model. Results show the positive impact of the GNSS-ZTD data assimilation on the forecast of synoptic-scale circulations and precipitation in spring and summer. Other studies followed in France (Boniface et al., 2009; Yan et al., 2009) and found a positive impact of GNSS-ZTD data assimilation on the NWP forecast.
- Bennitt and Jupp (2012) assimilated GNSS-ZTD observations by both 3DVar and 4DVar using the Met Office NAE. The assimilation of GNSS-ZTD resulted in an improvement of the cloud forecast.
- Lindskog et al (2017) performed GNSS-ZTD data assimilation into the HARMONIE-AROME model at 2.5 km horizontal resolution. The assimilation was performed by 3DVar and improved the forecast up to one and a half day.
- Rohm et al. (2019) assimilated GNSS (both ZTD and Precipitable Water) in the WRF model at 4 km horizontal resolution over Poland for two months. They found an improvement in predicting both water vapor and precipitation.

https://doi.org/10.5194/nhess-2023-18
Preprint. Discussion started: 22 February 2023


Natural Hazards and Earth System Sciences Discussions

- Giannaros et al. (2020) showed the positive impact of GNSS-ZTD data assimilation on both precipitation and water vapor forecast over Greece, and Caldas-Alvarez et al. (2020), showed similar results with the climatic setting of the COSMO model over a large portion of the Mediterranean and Central Europe.

Other works showed the positive impact of assimilating GNSS data for precipitation forecasts in different countries (Risanto et al., 2021; Singh et al., 2019; Trzcina et al., 2020; Yang et al., 2020).

The assimilation of GNSS data is also used in the operational context. The Rapid Refresh model over US assimilates GPS-derived Integrated Water Vapor (IWV) every hour from 300 stations across the US (Benjamin et al. 2016). The study shows that there is a clear benefit in using GNSS observations in rapid refresh weather forecast.

Considering the GNSS data assimilation over Italy, Faccani et al. (2005), using MM5 model at 9 km horizontal resolution and 3DVar to assimilate GNSS-ZTD over Italy, found improvements in the precipitation forecast during the transition from winter to spring.

By assimilating a wide range of Sentinel-1 and GNSS-ZTD observations in the WRF model, Lagasio et al. (2019) found that the forecasts benefit the most when the model is provided with information on the wind field and/or the water vapor content. Mascitelli et al. (2019, 2021) reported two successful experiments of GNSS-ZTD and Precipitable Water Vapor (PWV) data assimilation with the RAMS@ISAC model. The 3DVar was used to assimilate GNSS-ZTD, while nudging was used to assimilate the PWV. In both cases the assimilation showed a significant improvement in the short-term prediction of water vapor with smaller impact on the precipitation forecast.

This paper goes in a similar direction in the sense that it uses the GNSS-ZTD data assimilation to improve the precipitation and water vapor forecast over Italy. Compared to similar studies, however, it uses a longer period and/or a larger number of GNSS receivers widespread over the country, giving a robust assessment on the impact that GNSS-ZTD data assimilation can have on the forecast at the local scale.

This paper is organized as follows: Section 2 shows the data and methods used including the model setting, the GNSS-ZTD dataset, and the statistics for the verification. Section 3 discusses the results showing the impact of GNSS-ZTD data assimilation on the WRF analyses (both ZTD and PWV), on the precipitation forecast for a case study, and on the PWV and precipitation forecast for the whole period. Conclusions are given is Section 4. Finally, more details on the statistics used in the paper as well as the resampling test are reported in two appendices.

2 Data and methods

2.1 WRF model configuration and assimilation method

The model used in this study is the Weather Research and Forecasting with advanced WRF dynamic (WRF-ARW, Version 4.1.3, Skamarock et al., 2019). The model was run over one domain covering the whole Italian territory and the Central Europe (Figure 1) with a spatial horizontal resolution of 3km. The model grid has 635x635 grid points and 50 vertical levels, with the model top at 50 hPa. The main physical parameterization used are the following: the Thompson scheme (Thompson et al.

https://doi.org/10.5194/nhess-2023-18
Preprint. Discussion started: 22 February 2023

Natural Hazards and Earth System Sciences
Discussions

2008) for microphysics, the Mellor-Yamada-Janjic (Eta) TKE scheme for boundary layer (Janjic, 1994) the Dudhia scheme (Dudhia, 1989) and the Rapid Radiative Transfer Model (RRTM, Mlawer et al. 1997) for short wave and longwave radiation, respectively.

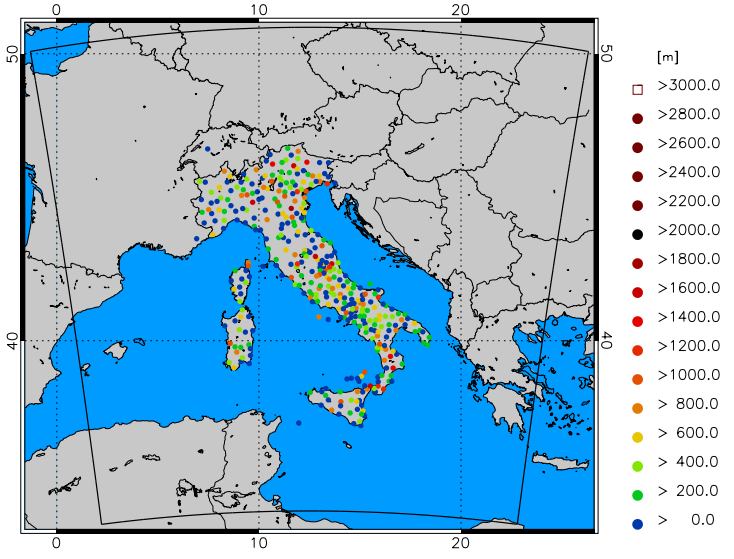

Figure 1: WRF model domain and GNSS receivers height ([m]) above sea level.

The experiment aims at evaluating the impact of GNSS-ZTD data assimilation on the precipitation prediction at the short-term (up to 6h in this paper). For this purpose, we considered a one-month period, from 02 to 31 October 2019. The choice of the period is due to two main reasons: on the one hand, this month was characterized by both widespread and localized precipitation events over Italy, on the other hand, a dense network of GNSS receivers (about 500) is available for the country. It is important to note that the number of receivers actually used for data assimilation was reduced to 388 by applying data thinning as discussed in Sect. 2.2.

GNSS-ZTD data assimilation was performed using the 3DVar tool distributed with WRF model, which is one of the components of WRFDA system, that includes also 4DVar and Ensemble data assimilation systems (Barker et al., 2004; Barker et al. 2012; Huang et al., 2009).

We consider two kinds of simulations: background simulations, without GNSS-ZTD data assimilation, hereafter also BCKG, and simulations assimilating GNSS-ZTD, hereafter also GPS.

The temporal scheme used for the simulations uses a Very Short-term Forecast (VSF) approach, with a 6h update (Figure 2).

https://doi.org/10.5194/nhess-2023-18
Preprint. Discussion started: 22 February 2023

Natural Hazards and Earth System Sciences
Discussions

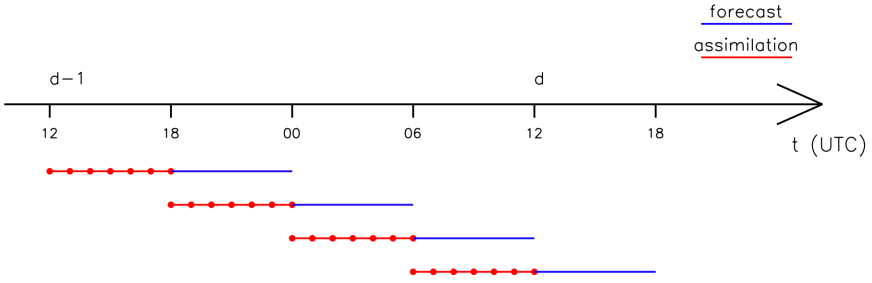

Figure 2: Rapid Update Cycle at 6h. Red dots denote analysis times.

In this scheme, for each day, we run four simulations starting from a cold start. Each simulation lasts 12 hours. The first 6h of each run are used for the model spin-up and for data assimilation (the latter for GPS simulations only), while the last 6h are used as forecast. Therefore, 4 runs are necessary to cover a whole day. The European Centre for Medium range Weather Forecast (ECMWF) Integrated Forecast System (IFS) 3-hourly operational analysis/forecast cycle at 0.25° starting at 12 UTC on the day before the actual day to forecast is used for initial and boundary conditions, to simulate a real forecasting context. In the assimilation phase, we considered an analysis every 1 hour (red points of Figure 2), starting from the beginning of the simulation and reaching the 6th hour, so a total of 7 analyses are performed for each run.

GNSS-ZTD observations are assimilated by 3DVar, which is a variational approach involving the calculation of the analysis that minimizes a cost function by measuring its distances from background and observations. The cost function is given by:

$$J(x) = \frac{1}{2}(\boldsymbol{x} - \boldsymbol{x_b})^T \boldsymbol{B}^{-1}(\boldsymbol{x} - \boldsymbol{x_b}) + [\mathbf{y_o} - H(\boldsymbol{x})]^T \boldsymbol{R}^{-1}[\mathbf{y_o} - H(\boldsymbol{x})]$$

where $\boldsymbol{x}$ is the state vector, $\boldsymbol{x_b}$ is the background field, H is the forward observational operator which transforms the $\boldsymbol{x}$ vector in the observational space, $\boldsymbol{y_o}$ is the observations vector, $\boldsymbol{B}$ and $\boldsymbol{R}$ are the error covariance matrices, respectively for background and observations.

The $\boldsymbol{R}$ matrix is given by the sum of instrumental and representation errors. To prepare observational data for 3DVar, the OBSPROC tool was employed for GNSS-ZTD observations. Data for each analysis were considered on a 1-hour time range, centered at the hour of the analysis. The $\boldsymbol{R}$ matrix is diagonal, which requires data thinning (see next section), and the ZTD error is set to 5 mm.

As regards the $\boldsymbol{B}$ matrix, the calculation for this study is performed via the GEN_BE tool, employing the NMC method (Parrish and Derber, 1992) for the month of October and the option CV5, which accounts for five control variables.

2.2 Observational datasets and verification procedure

2.2.1 GNSS data

To achieve a good spatial density of the ZTD measurements, the GNSS data have been collected from all major Italian national and regional GNSS networks. To derive ZTDs, GPS L1 and L2 pseudorange and phase measurements were adjusted in PPP

https://doi.org/10.5194/nhess-2023-18
Preprint. Discussion started: 22 February 2023


Natural Hazards and Earth System Sciences Discussions

mode (Bevis et al., 1992; Zumberge et al., 1997), by using the GNSS data processing suite Breva, developed by GReD, based on the open-source software goGPS (Herrera et al., 2016).

Several of the used stations tracked only GPS satellites, thus we decided to process only GPS observations, disregarding data from other GNSS constellations. Table 1 describes the corrections applied to the observations, as well as the stochastic model.

Table 1: Corrections applied to the observations and stochastic model.

Ionospheric delay	Pre-eliminated through the iono-free linear combination of L1 and L2
Ephemerides	IGS final combination
Coordinates	Estimated, one set per station per day
ZTD	Estimated epoch wise, with random walk model (noise 0.003 $m/\sqrt{h}$)
ZTD North and East gradient	Estimated epoch wise, with random walk model (noise 0.0001 $m/\sqrt{h}$)
Solid Earth	Corrected according to IERS 2010
Ocean loading effects	Corrected using coefficient computed from FES 2004 model
Mapping function	Vienna Mapping Function

Figure 1 presents the locations and the heights of the 388 GNSS stations used over the Italian peninsula and its surroundings after a reduction of their number. Although the initial number of GNSS receivers was about 500, more than 100 GNSS receivers were discarded considering the following two requirements: a) the difference between the receiver and WRF model height at the closest grid point to the GNSS receiver must be less than 300 m (similarly to Bennitt and Jupp, 2012; Rohm et al., 2019; and Mascitelli et al., 2019) and b) in case two or more receivers fell in the same WRF grid cell, the one whose height was closer to the model orographic height was retained. At the end of the process, 388 GNSS receivers were used for data assimilation and the closest distance between any two receivers was larger than 10 km. No further data thinning was applied.

2.2.2 Forecast verification

As regards the evaluation of the precipitation forecast performances, five precipitation scores are calculated, i.e. Frequency Bias (FBIAS), Probability of Detection (POD), Threat Score (TS), Equitable Threat Score (ETS) and False Alarm Rate (FAR). A detailed description of these scores is provided in Appendix A.

In the following, we will show the results of the scores summarizing them through the Performance Diagram (Roebber, 2009), with the exception of ETS. In this diagram the perfect score is the one that reaches the upper right corner of the diagram. The x-axis represents the Success Ratio (SR) which is defined as 1-FAR, while the POD is on the y-axis. The straight lines from the origin represent the FBIAS while the hyperboles branches are the TS.

https://doi.org/10.5194/nhess-2023-18
Preprint. Discussion started: 22 February 2023


Natural Hazards and Earth System Sciences
Discussions

We considered the forecast for both types of run, BCKG and GPS, taking into account two main periods after the last analysis time, in order to evaluate the impact of GNSS-ZTD data assimilation on the precipitation forecast at different ranges: the first 3h (from the 6th to the 9th hour of run) and the second 3h of forecast (from the 9th to the 12th of run). Model forecast in correspondence of a given rain gauge is computed using the nearest-neighbour method. By this method, we consider all WRF precipitation values at grid points in a radius of $2\Delta x\sqrt{2}$ from the rain gauge, Δx being the WRF model grid spacing, and we select the grid point with closest rainfall value to the rain gauge observation.

Precipitation data come from the Italian rain gauge network, with more than 4000 rain gauges over Italy. This network belongs to the Italian regional administrations and data are collected nationwide by the Department of Civil Protection (Davolio et al., 2015).

Furthermore, a test to assess the statistical significance of the differences between BCKG and GPS precipitation forecasts is performed. The resampling test of Hamill (1999) is used (see Appendix B for details).

For precipitable water vapor verification, we focused on both the assimilation and forecast phases. Verification is made calculating two main scores:

- BIAS, which measures the mean differences between forecast (F) and observation (O):

$$BIAS = \frac{1}{N}\sum_{i=1}^{N}(F_i - O_i) \quad (1)$$

- Root Mean Square Error (RMSE), which measures the mean of the squared differences between forecast and observation:

$$RMSE = \sqrt{\frac{1}{N}\sum_{i=1}^{N}(F_i - O_i)^2} \quad (2)$$

with *N* number of forecast-observation pairs considered in the statistics.

3 Results and discussion

3.1 ZTD and precipitable water vapor results for the analysis phase

In this section we consider the differences between the first guess (FG) and the observations, and between the analyses (ANL) and the observations. Statistics are presented considering all simulations (30*4). For each simulation, six times are considered for first guess and analysis, one for each time (red dots of Figure 2), except for the analysis at the initial time of each simulation because it is coincident with the last analysis time of the previous simulation, the latter being considered in the results.

Two types of statistics are shown. In the first statistics we present the time series of the BIAS and RMSE errors aggregating all receives together for each analysis time; in this case, referring to the Eqn. (1) and (2), N is the number of GNSS receivers considered at the analysis time. In the second statistics, we show the PWV BIAS and RMSE computed for each receiver; in

https://doi.org/10.5194/nhess-2023-18
Preprint. Discussion started: 22 February 2023

Natural Hazards and Earth System Sciences
Discussions

this case, referring to Eqn. (1) and (2), N is the number of analyses done for the whole period (30*4*6=720 first guess and analysis pairs).

Figure 3 shows the time series for ZTD BIAS (Figure 3a) and ZTD RMSE (Figure 3b) calculated for the whole period. From Figure 3a it is apparent that the ANL BIAS (blue curve) has lower absolute values compared to that of FG (red curve) for all times considered. The better results obtained by ANL is confirmed also by the BIAS values calculated over all times together, shown in the upper right part of the figure, which is halved after the analysis (BIAS_A, -0.1 cm) compared to the first guess (BIAS_F, -0.2 cm). Interestingly, the WRF first guess bias is mainly negative showing an underestimation of the water vapor content in the atmosphere. This underestimation is reduced by GNSS-ZTD data assimilation that increases the water vapor in the model. The positive impact of the GNSS-ZTD data assimilations is confirmed by the RMSE calculation (Figure 3b). The RMSE for the whole period for the analyses (RMSE_A) is 0.7 cm, compared to the value of 1.3 cm for the first guess (RMSE_F).

a)

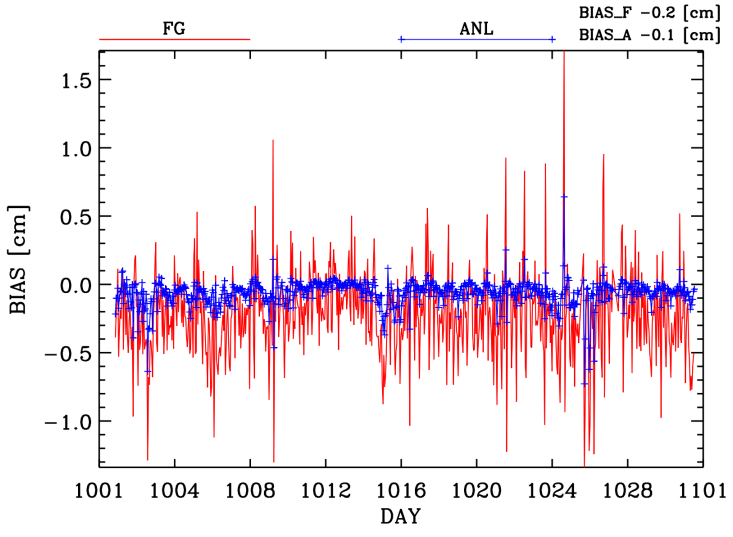

b)

https://doi.org/10.5194/nhess-2023-18
Preprint. Discussion started: 22 February 2023

Natural Hazards and Earth System Sciences
Discussions

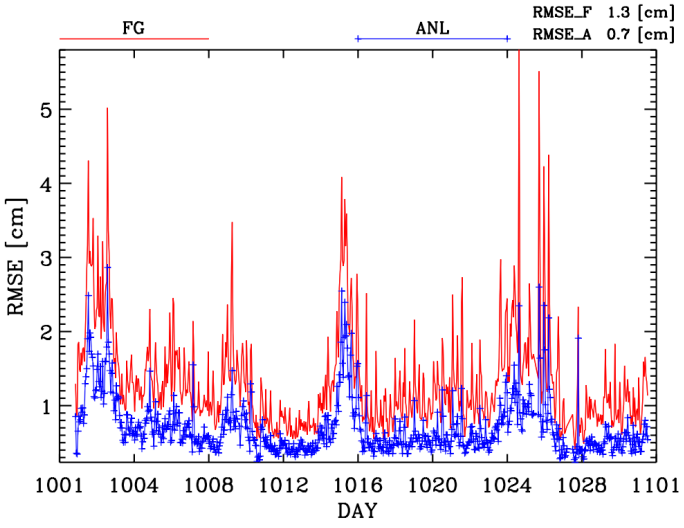

Figure 3: Time series of ZTD BIAS (a) and of ZTD RMSE (b) calculated for all sensors together for first guess (red curve) and analysis (blue curve) during the analysis phase. Dates are shown along the x-axis.

It is important to discuss the impact of GNSS-ZTD data assimilation over the Italian territory. This is shown considering the PWV estimated by the ZTD. The PWV in millimeters is given by:

$$PWV = Q(ZTD_{GNSS} - ZHD_{WRF})$$

where ZHD_{WRF} is the hydrostatic delay calculated using the Saastamoinen (1972) equation given the WRF surface pressure (p_{sfc}), latitude (ϕ) and height (h):

$$ZHD_{WRF} = \frac{0.0022767 p_{sfc}}{1.0 - 0.0266\cos(2\phi) - 0.00000029\,h}$$

The proportionality factor Q is computed as follows:

$$Q = \frac{10^6}{R_W(\frac{k_3}{T_m} + k_2')}$$

where R_w=461 J/(kgK) is the gas constant for water vapor, k_2'=22.9726 K/hPa and k_3=375463 K^2/(hPa) are the refractivity constants from Reuger (2002) and T_m is the mean temperature given by:

$$T_m = 70.2 + 0.72 T_{WRF}$$

where T_{WRF} is the WRF surface temperature.

Figure 4 shows the PWV RMSE (panels a) and b), for first guess and analysis, respectively) and the BIAS (panels c) and d) for first guess and analysis, respectively) for the whole period at each GNSS receiver. Both statistics are improved by data assimilation. The impact of GNSS-ZTD data assimilation on PWV RMSE is apparent as most of the green-orange-red colors (RMSE between 1.0 and 2.5 mm, Figure 4a) are reduced to dark green-green colors (RMSE between 0.5 and 1.5 cm, Figure 4b).

https://doi.org/10.5194/nhess-2023-18
Preprint. Discussion started: 22 February 2023

Natural Hazards and Earth System Sciences
Discussions

For the BIAS the improvement is less apparent, but it is clearly shown by the increase of the orange, red and yellow dots in panel d) compared to panel c) of Figure 4.

a)

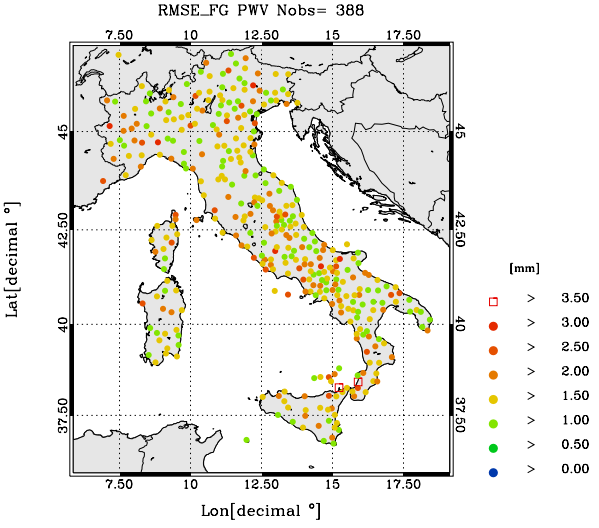

b)

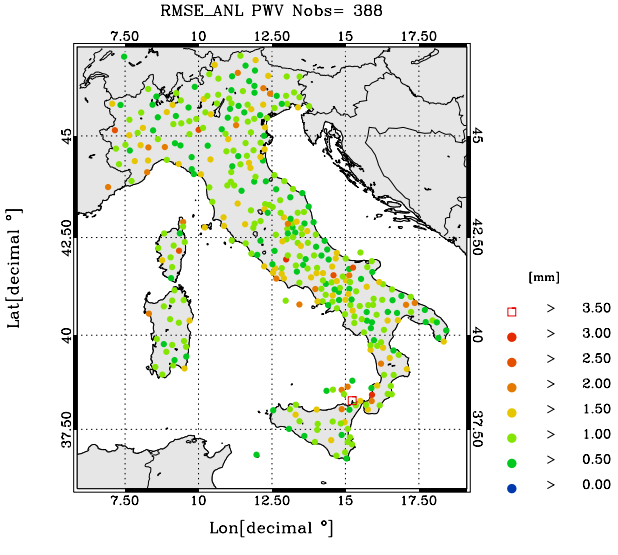

c)

https://doi.org/10.5194/nhess-2023-18
Preprint. Discussion started: 22 February 2023

Natural Hazards and Earth System Sciences
Discussions

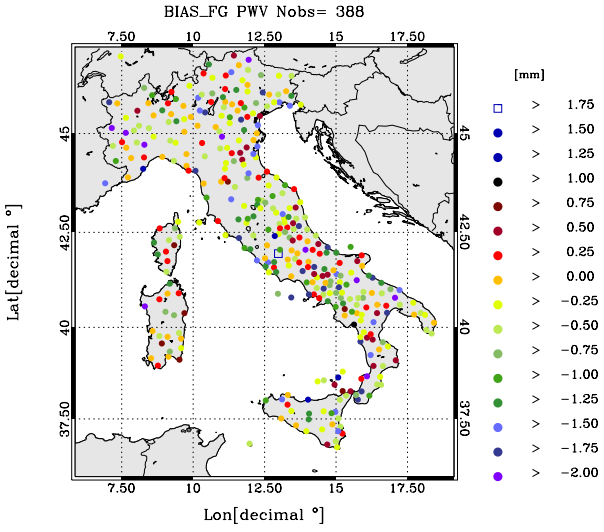

d)

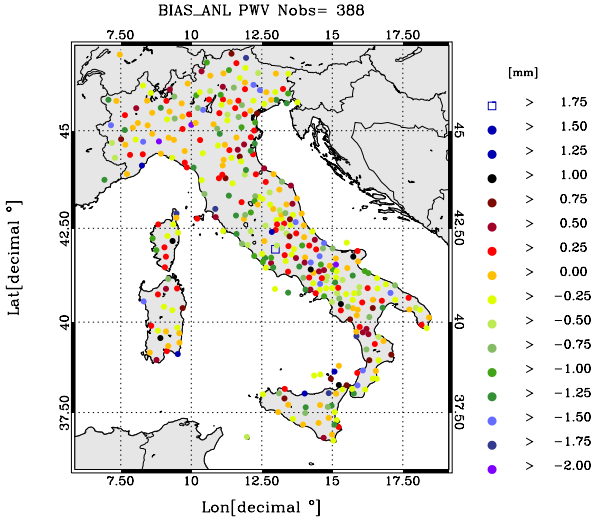

Figure 4: PWV RMSE for FG (a) and ANL (b) and PWV BIAS for FG (c) and ANL (d) calculated for each sensor over all times of analysis.

All in all, the results of this section show a positive impact of GNSS-ZTD data assimilation on the ZTD and PWV over the period, and the net result is the increase of the model water vapor content over the area, because the first guess underestimation of the ZTD (and PWV) is reduced by data assimilation.

https://doi.org/10.5194/nhess-2023-18
Preprint. Discussion started: 22 February 2023

Natural Hazards and Earth System Sciences
Discussions

3.2 Rainfall forecast for a case study

The selected date is the 15 October 2019, in the 3 hours between 18 and 21 UTC. This phase was selected because it is representative of the improvement that the assimilation of GNSS-ZTD had for several cases on the 3h precipitation forecast. During this time period, three main thunderstorms developed: the first two over the North-East and North-West of Italy, respectively, with a precipitation maximum between 60 and 70 mm/3h, and the third in Southern Italy, with precipitation ranging between 40 and 50 mm/3h. We start examining the innovations, i.e. the analysis minus first guess fields, at 18 UTC on 15 October (Figure 5a) because the precipitation between 18 and 21 UTC is predicted just after the 18 UTC analysis, and some correspondence between the analysis and the precipitation forecast is found.

Figure 5a shows the innovations at 18 UTC on 15 October 2019 at about 1800 m above the ground surface. A complex pattern of positive and negative innovations is shown thanks to the many observations available, which add information on the water vapor field at the subregional scale (the distance between two closest maxima or minima of Figure 5a can be roughly estimated in 50-70 km).

Figure 5b shows the latitude-height cross section of the innovations at the same time of Figure 5a. The cross section is for the longitude 12.6°E. Water vapour values in the range 0.4-1.0 g/kg are shown in several parts of the cross section at about 1600 m height a.g.l. in western Sicily (37.5 °N) revealing a considerable impact of GNSS-ZTD data assimilation (> 10% of the first guess value) on the water vapor field.

a)

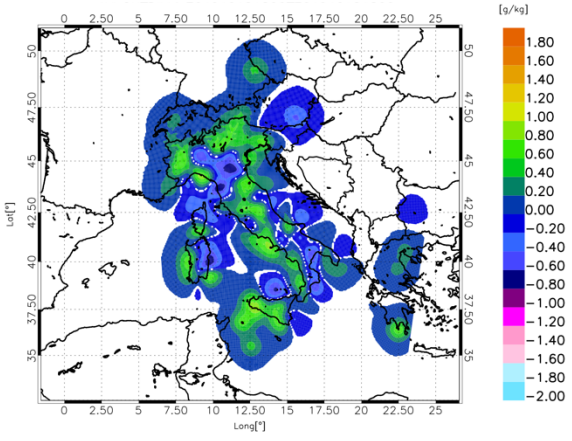

b)

https://doi.org/10.5194/nhess-2023-18
Preprint. Discussion started: 22 February 2023

Natural Hazards and Earth System Sciences
Discussions

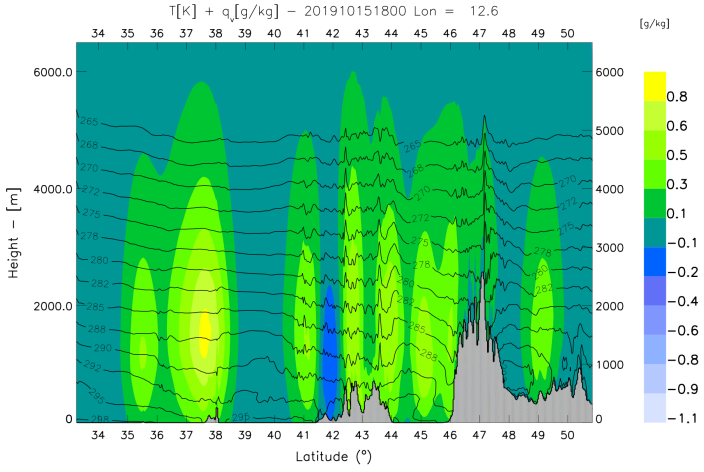

Figure 5: Innovations of water vapor at 18 UTC on 15 October 2019; a) horizontal map around 1800 m above the surface; b) latitude-height cross-section of water vapor innovations with the first guess temperature (black contours).

Between 18 and 21 UTC, moderate to intense precipitation are shown in NE and NW of Italy by rain gauge observations, with maximum intensities larger than 60 mm/3h (Figure 6a). Some areas of moderate precipitation are apparent in Central and Southern Italy with maxima between 20 and 50 mm/3h.

The BCKG, Figure 6b, has a good forecast because it represents the two main precipitation areas over NW and NE of Italy. There are, however, less satisfactory points in the BCKG rainfall forecast: first, the maximum over NE of Italy is composed by two branches and one of them is displaced close to the sea, starting from Venice and going toward NE. This branch is a false alarm, at least in its southernmost part. Second, the maximum over Central Italy, starting from Tuscany and displaced in the SW-NE direction is displaced to the North, compared to observations. Third, the precipitation over Southern Italy is missed.

The assimilation of GNSS-ZTD improves the precipitation forecast. The pattern of the precipitation over NE is more in agreement with observations because precipitation does not appear separated in two branches as in the BCKG and the precipitation amount for GPS simulations is higher, better catching the observation maximum. This agrees with the increase of the water vapor over NE of Italy given by the last assimilation (Figure 5a). A similar improvement is apparent in the South of Italy, where the precipitation was missed by the BCKG. In this case the observed precipitation is well forecast by GPS and the increase of precipitation is determined by the increase of water vapor over the area (Figure 5a). The maximum over Central Italy is not much improved by the assimilation of GNSS-ZTD because, even if there is better superposition with observations compared to the background, there are more false alarms in the GPS forecast.

a)

https://doi.org/10.5194/nhess-2023-18
Preprint. Discussion started: 22 February 2023

Natural Hazards and Earth System Sciences
Discussions

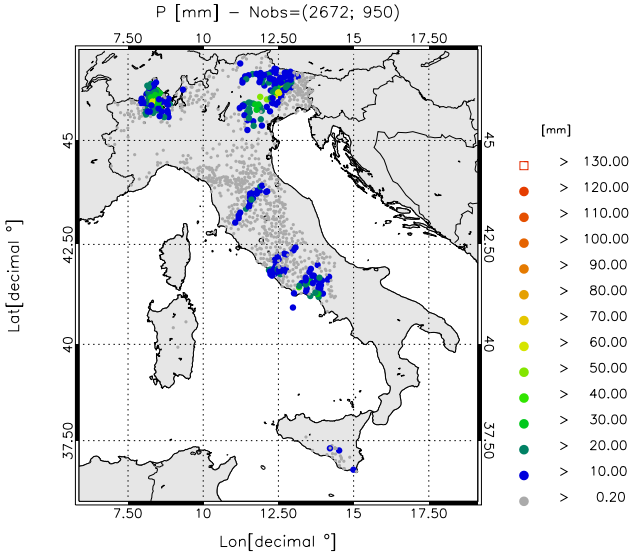

b)

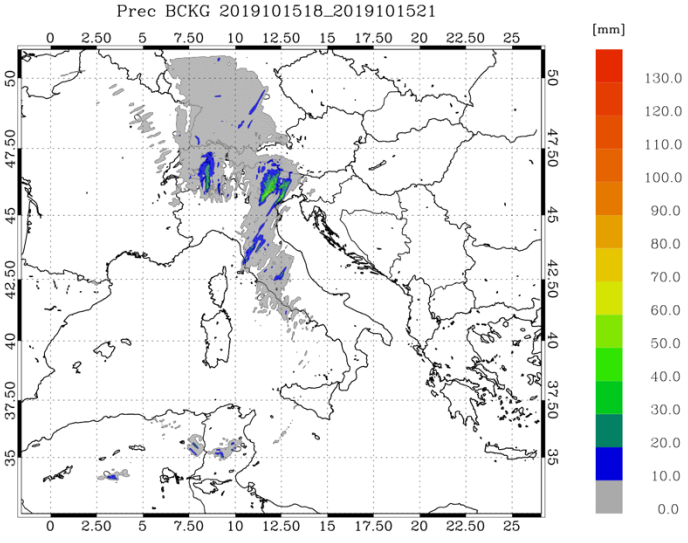

c)

https://doi.org/10.5194/nhess-2023-18
Preprint. Discussion started: 22 February 2023

Natural Hazards and Earth System Sciences
Discussions

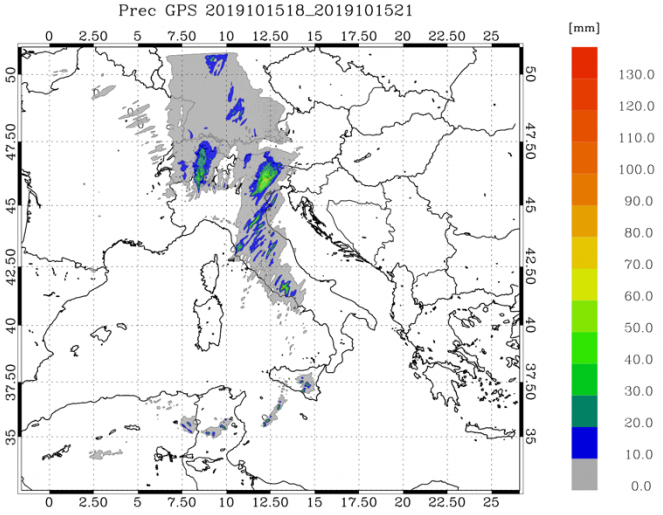

Figure 6: Precipitation between 18 and 21 UTC on 15 October 2019: a) Rain gauges observations; b) BCKG forecast; c) GPS forecast.

3.3 Results for the water vapor forecast for the whole period

In this section we show the impact of GNSS-ZTD data assimilation on the PWV forecast. Three different statistics are considered: the time series of the differences between the PWV RMSE of BCKG and GPS simulations for different forecasting times; the time series of the difference between the PWV absolute value of the BIAS of BCKG and GPS simulations for different forecasting times; the RMSE maps of PWV for BCKG and GPS on two different forecasting times. The PWV is computed as shown in Sect. 3.1, replacing ZTD_{GNSS} with ZTD_{WRF}.

The first two statistics are shown in Figure 7 for the first (red curve), third (blue curve) and sixth hour of forecast (green curve). Considering the differences between BCKG and GPS PWV RMSE, positive values show better performance of the forecasts assimilating GNSS-ZTD and, from Figure 7a, it is apparent that the GNSS-ZTD data assimilation improves the PWV forecast at different forecast ranges, with the exceptions of few cases. The RMSE of the GPS simulations can have a RMSE lower than BCKG simulations up to 2.5 mm and, from Figure 7a, it is also notable a decrease of the improvement of GNSS-ZTD data assimilation for longer forecasting times as the red curve shows, with some exceptions, larger values than the blue curve, which, in turn, has larger values that the green curve. However, it is important to note that the positive impact of GNSS-ZTD data assimilation on the PWV forecast is still apparent after six hours of forecast.

The bias is also improved by the GNSS-ZTD data assimilation as the difference of the absolute value of the bias for BCKG and GPS simulations shows positive values. As for RMSE, the bias improvement decreases with forecasting time.

a)

https://doi.org/10.5194/nhess-2023-18
Preprint. Discussion started: 22 February 2023

Natural Hazards and Earth System Sciences
Discussions

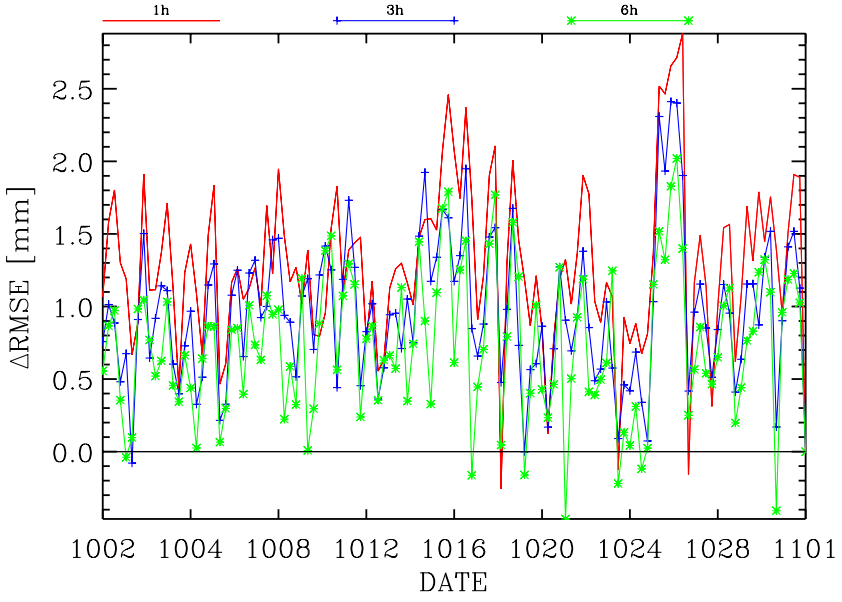

b)

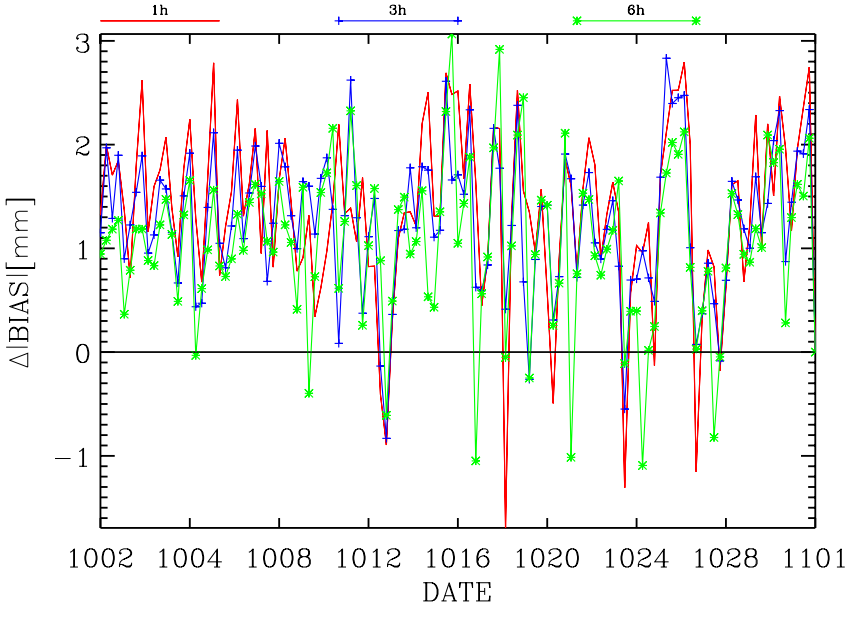

Figure 7: Time series of the differences between PWV-RMSE for BCKG and GPS (a) and of the difference of the absolute value of the Bias for the BCKG and GPS simulations (b). Red curve is for the first forecast hour, blue curve is for the 3rd forecast hour and the green curve is for the 6th forecast hour.

https://doi.org/10.5194/nhess-2023-18
Preprint. Discussion started: 22 February 2023

Natural Hazards and Earth System Sciences
Discussions

It is interesting to evaluate the spatial distribution of the improvement of GNSS-ZTD data assimilation on the PWV forecast over Italy. This is shown in Figure 8 for the first hour of forecast (panels a) and b) for BCKG and GPS, respectively) and for the sixth hour of forecast (panels c) and d) for BCKG and GPS, respectively). Figure 8 shows that the improvement of RMSE is not limited to a specific area, thanks to the good coverage of the GNSS receivers used in this work, but it is widespread with RMSE more than halved in correspondence of most receivers.

The RMSE for the sixth forecast hour increases for both BCKG and GPS simulations compared to the first forecast hour, as expected because the forecast error increases with forecasting time. However, the increase of the RMSE error is larger for the GPS simulations (comparison between panels b) and d)) than for the BCKG simulation (panels a) and c)), and the impact of GNSS-ZTD data assimilation decreases with the forecasting time over the whole Italian territory.

a)

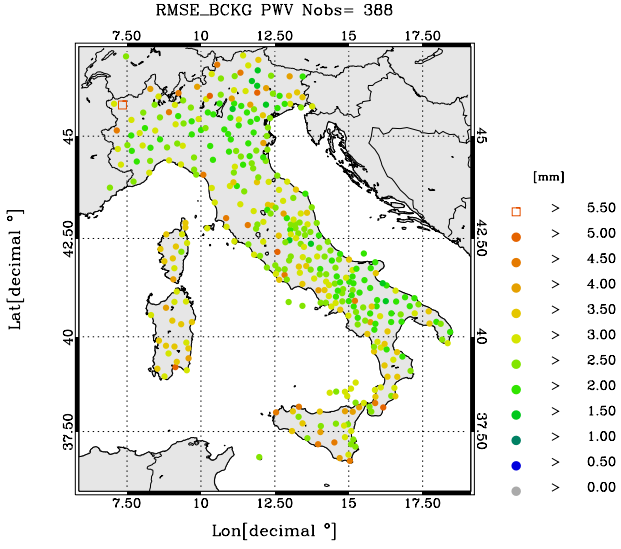

b)

https://doi.org/10.5194/nhess-2023-18
Preprint. Discussion started: 22 February 2023

Natural Hazards and Earth System Sciences
Discussions

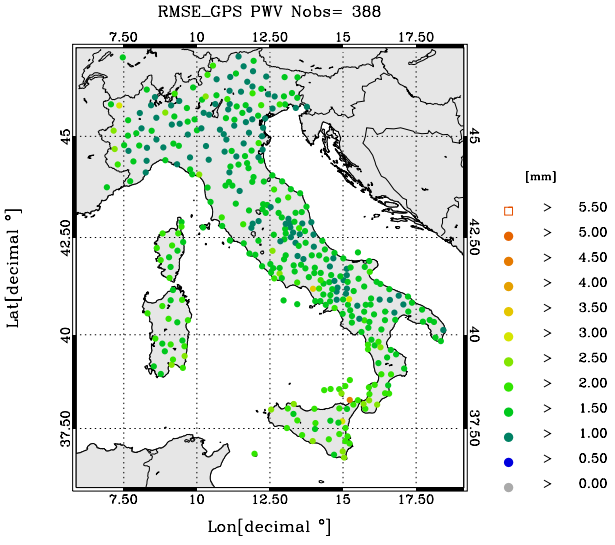

335

c)

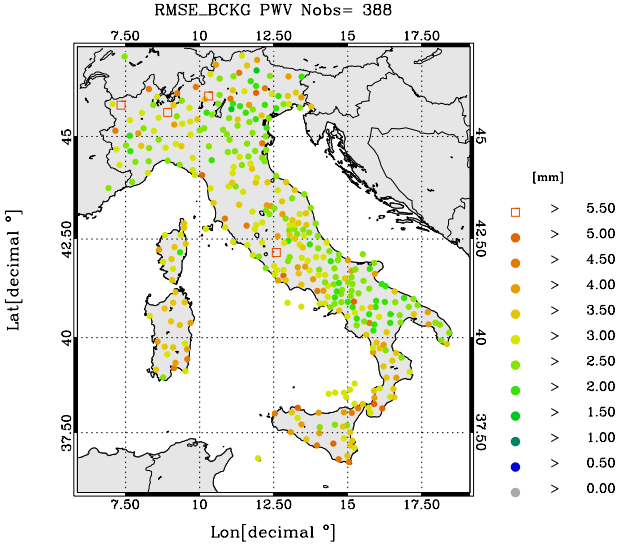

d)

https://doi.org/10.5194/nhess-2023-18
Preprint. Discussion started: 22 February 2023

Natural Hazards and Earth System Sciences
Discussions

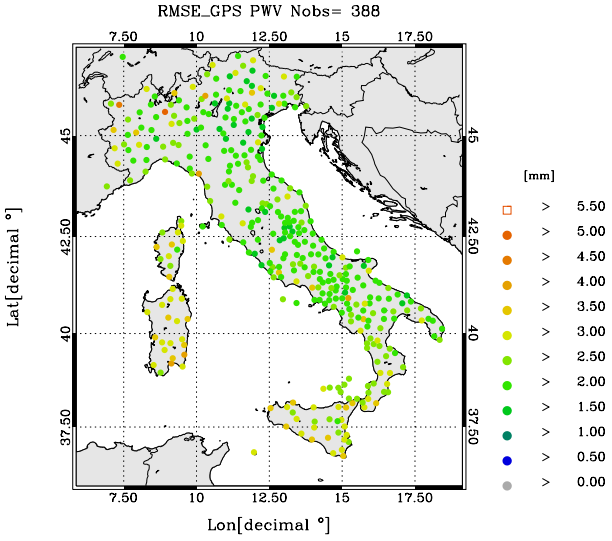

Figure 8: Maps of the PWV RMSE for the first (a, b) and sixth (c, d) forecasting hour. Panels a) and c) are for BCKG simulations, panels b) and d) are for GPS simulations.

3.4 Results for the precipitation forecast over the whole period

In this section we show the impact of GNSS-ZTD data assimilation on the precipitation forecast statistics for the whole period (2-31 October 2019). Two precipitation phases are considered: the first 3h of each simulation after the last assimilation time (also 0-3h) and the following 3h, i.e. from the 3rd to the 6th hour of each simulation after the last assimilation time (hereafter 3-6h), to evaluate for how long the GNSS-ZTD data assimilation impacts the precipitation forecast.

Performance diagrams are shown in Figure 9 for both BCKG and GPS and for three different precipitation thresholds, namely 1 mm/3h, 10 mm/3h and 30 mm/3h. Starting from the analysis of the 0-3h forecast, the following four points can be noticed: a) the GNSS-ZTD assimilation improves the precipitation forecast for all precipitation thresholds as the GPS symbols are always closer to the upper right corner compared to the BCKG; b) the FBIAS of the BCKG is underestimated for all precipitation thresholds; c) the FBIAS, POD, FAR and the TS of the GPS are always larger than the corresponding BCKG; d) the performance of both GPS and BCKG decreases with the increasing precipitation thresholds. The point a) shows that the precipitation forecast is improved by GNSS-ZTD data assimilation; the points b) and c) show that the assimilation of GNSS-ZTD improves the BCKG underestimation of the precipitation events for all thresholds. The point c) shows that, while the performance of GPS is improved compared to BCKG, the added value of GNSS-ZTD data assimilation is reduced by the FAR increase. This point will be confirmed by the results of the statistical test shown later in this section. The point d) shows the well-known difficulties to correctly predict the correct amount, location, and timing of precipitation events as their intensity increases.

Results for the 3-6h phase are like those of the 0-3h period, highlighted in the four points above, with the exception that the FAR for the 30 mm/3h threshold is reduced by GNSS-ZTD data assimilation. In addition, the comparison of Figures 9a and

https://doi.org/10.5194/nhess-2023-18
Preprint. Discussion started: 22 February 2023

Natural Hazards and Earth System Sciences
Discussions

9b shows that the improvement of the model performance decreases with increasing forecasting time because the GPS and BCKG symbols are closer for the 3-6h phase compared to the 0-3h forecast. This is in agreement with the analysis of the PWV presented in the previous section.

All in all, there are two important points to remark for the 0-3h and 3-6h performance diagrams: a) the performance of BCKG is improved by GNSS-ZTD data assimilation; b) the impact of assimilating GNSS-ZTD on the precipitation forecast lasts at least 6h.

a)

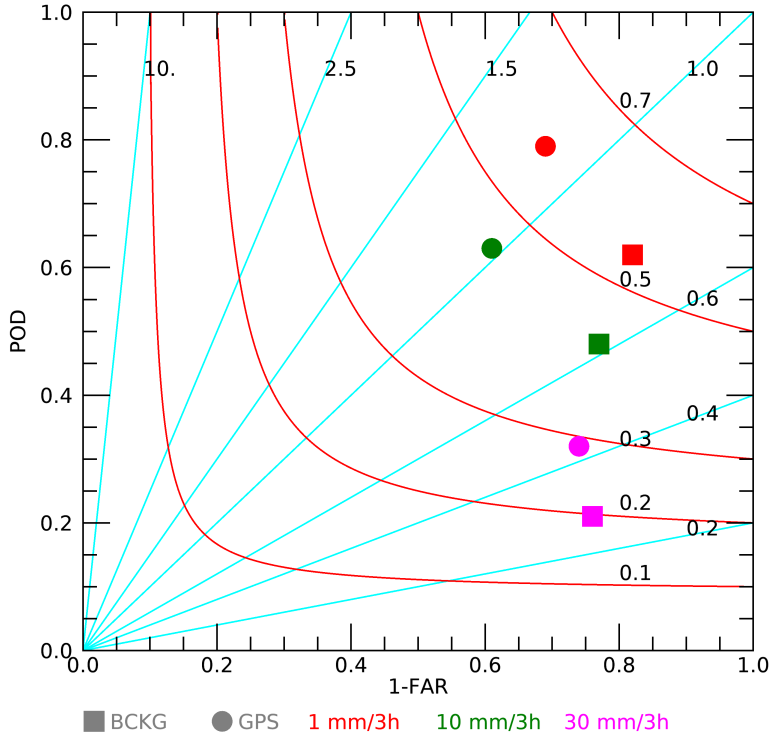

b)

https://doi.org/10.5194/nhess-2023-18
Preprint. Discussion started: 22 February 2023

Natural Hazards and Earth System Sciences
Discussions

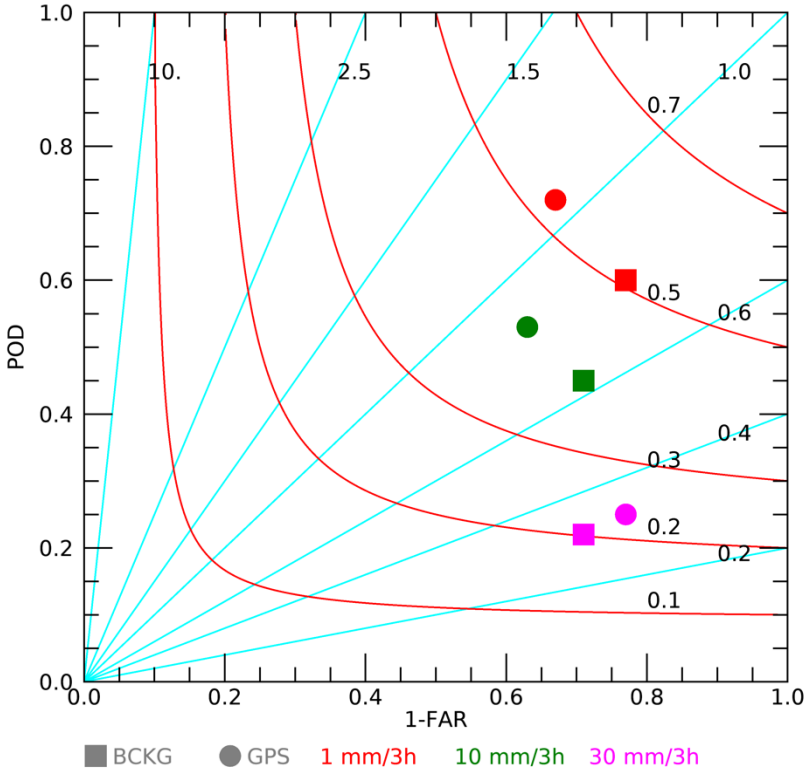

Figure 9: Performance diagram showing precipitation scores over the whole period for BCKG (squares) and GPS (circles) for the 0-3h period (a) and for the 3-6h period (b) after the assimilation phase for three different precipitation thresholds: 1 mm/3h (in red), 10 mm/3h (in green) and 30 mm/3h (in magenta).

To better examine the difference of the statistical scores of the BCKG and GPS forecasts shown in Figure 9, the results of a bootstrap statistical test (see Appendix B for details) are shown in Table 2 for the 0-3h and 3-6h forecast phases. The level of statistical significance is shown in plain text (90, 95, 99%) if the GPS simulations perform better than BCKG, in bolded italic for the opposite case. The statistical test was computed for 1mm/3h, 5mm/3h and then every 5mm/3h up to 50 mm/3h thresholds. Results are shown up to 30 mm/3h thresholds because differences were not statistically significant for larger precipitations. From Table 2, it is apparent that the assimilation of GNSS-ZTD has a good and significant impact on the precipitation forecast because FBIAS and POD are improved for several thresholds. The FAR is worsened by the data assimilation because of the larger number of false alarms predicted by GPS compared to BCKG. This limits the improvement of ETS, which accounts for both hits and false alarms; however, the ETS has statistically significant improvements at 25 and 30 mm/3h showing a significant and positive impact of GNSS-ZTD data assimilation for moderate-intense precipitation forecast. It is finally noticed the improvement of the FBIAS, POD, and ETS scores for both 0-3h and 3-6h phases, showing that the impact of GNSS-ZTD data assimilation lasts at least 6h into the forecast.

https://doi.org/10.5194/nhess-2023-18
Preprint. Discussion started: 22 February 2023

Table 2: Results of the resampling statistical test. Statistical significance of 90, 95 and 99% is shown in plain-text when GNSS-ZTD data assimilation improves the statistics, while it is shown in bolded italic when the GNSS-ZTD data assimilation has a negative impact on the statistics. Significant values less than 90% are not shown. The first number in each cell refers to the first 3h of forecast (0-3h), while the second number refers to the second 3h of forecasts (3-6h).

	1mm/3 h	5mm/3 h	10mm/3 h	15mm/3 h	20mm/3 h	25mm/3 h	30mm/3 h
FBIAS	99;99	99;99	99;99	99;/	99;/	95;90	95;/
ETS	90;/	/;/	/;/	/;/	/;/	90;90	95;/
POD	99;99	99;99	99;99	99;/	99;/	90;90	95;/
FAR	***99;99***	***99;95***	***99;/***	***95;/***	***90;/***	/;/	/;/

4 Conclusions

In this paper we studied the impact of GNSS-ZTD data assimilation on the short-term (up to 6h) forecast over Italy for the month of October 2019, using the WRF model. A dense dataset of 388 GNSS receivers was used.

The comparison between first guess and ZTD observations showed that the forecast without data assimilation underestimates the water vapor content for the period. The GNSS-ZTD data assimilation partially compensates for this underestimation increasing the water vapor content in the atmosphere. The data assimilation roughly halves both the BIAS and the RMSE statistics for the ZTD. The analysis over the Italian territory shows a general reduction of BIAS and RMSE of the PWV thanks to the rather homogeneous and widespread coverage of GNSS receivers.

A case study on 15 October 2019 was chosen to show the impact of assimilating GNSS-ZTD on the precipitation forecast. The analysis at 18 UTC shows that 3DVar spreads the water vapor innovations both horizontally and vertically, and the improvement of the short-term precipitation forecast is notable, the main drawback being the increase of false alarms over Central Italy.

Considering the statistics over the whole period, the analysis of the PWV forecast shows a clear improvement for the simulations with data assimilation. This improvement is widespread over the Italian territory. The PWV RMSE is almost halved for the first forecasting time. As expected, the improvement of the PWV RMSE decreases with forecasting time as the effects caused by data assimilation are partially advected out of Italy.

Assimilating GNSS-ZTD increases the precipitation of the short-term forecast compared to BCKG, which shows a systematic underestimation of the FBIAS. Two 3h periods were considered after the last analysis time: 0-3h and 3-6h. For both periods, the FBIAS and the POD are increased by data assimilation and the background forecast is improved. As a drawback, the number of false alarms was increased by GNSS-ZTD data assimilation. ETS is also improved by data assimilation, even if the increase in the number of false alarms limits the impact of data assimilation on this score.

https://doi.org/10.5194/nhess-2023-18
Preprint. Discussion started: 22 February 2023


Natural Hazards and Earth System Sciences Discussions

The results of the resampling statistical test show that the improvement for the FBIAS and POD are statistically significant for several thresholds up to 30 mm/3h. The FAR increase is statistically significant up to 20 mm/3h, while ETS has significant improvements for 1, 25 and 30 mm/3h.

All in all, the statistical analysis reveals a positive impact of GNSS-ZTD and the improvement is apparent up to 6h.

While the results of this paper are encouraging, there are several points that need future studies. First, the Mediterranean climate has an important seasonal variability and the impact of assimilating GNSS-ZTD must be studied in different seasons. Second, this study refers to only one month: longer periods must be considered to give a more robust assessment of the impact of GNSS-ZTD data assimilation on the forecast over Italy. Third, other techniques to assimilate GNSS data, as assimilating the precipitable water vapor (PWV) and the sensitivity of the results to the background error matrix and to the data thinning should be considered in future studies. Fourth, assimilating GNSS-ZTD in real-time over Italy and assimilating the ZTD gradients are two subjects that deserves detailed future research.

Acknowledgments

This work was realized in the project AEROMET (AERO spatial data assimilation for METeorological weather prediction) funded by the Lazio region - FESR Fondo Europeo di Sviluppo Regionale Programma Operativo regionale del Lazio. ECMWF is acknowledged for providing the computational resources for this work.

Appendix A: Precipitation scores

Scores are computed starting from contingency tables (Table A1) for dichotomous events, i.e. events that can have only two values. In this case the two values are “yes” or “no” and the event is: ‘‘precipitation is above or equal a certain threshold”.

Table A1. Contingency table for dichotomous events.

		Forecast	
		Yes	No
Observation	Yes	*a*	*c*
	No	*b*	*d*

In Table A1, *a, b, c* and *d* have the following meaning:

- *a* represents the hits. A hit occurs when both the precipitation forecast and the corresponding rain gauge observation are above or equal to a rainfall threshold;
- *b* represents the false alarms. A false alarm occurs when the precipitation forecast is above or equal to a rainfall threshold, while the corresponding rain gauge observation is below the same threshold;

https://doi.org/10.5194/nhess-2023-18
Preprint. Discussion started: 22 February 2023


Natural Hazards and Earth System Sciences Discussions

- *c* represents the misses, i.e. when the precipitation forecast is below a rainfall threshold, while the corresponding rain gauge observation is above or equal to the same threshold;
- *d* represents the correct no forecasts, i.e. when both the precipitation forecast and the corresponding observation are below a rainfall threshold.

Starting from the values in Table A1, the following scores can be defined:

- Frequency Bias (FBIAS)

$$FBIAS = \frac{a+b}{a+c}$$

which represents the frequency of the predicted events above a rainfall threshold with respect to observed events and can assume values between 0 and ∞, 1 being the best value possible.

- Probability of Detection (POD):

$$POD = \frac{a}{a+c}$$

which is the ratio between the number of correctly predicted events and the number of observed events and can assume values between 0 and 1, with 1 the best value possible.

- Threat Score (TS):

$$TS = \frac{a}{a+b+c}$$

which is given by the ratio between the number of events correctly predicted and the sum of observed and predicted events. TS assumes values between 0 and 1, and 1 is the best value that can be obtained.

- Equitable Threat Score (ETS):

$$ETS = \frac{a-a_r}{a+b+c-a_r}, \qquad \text{where } a_r = \frac{(a+b)(a+c)}{a+b+c+d}$$

ETS is similar to TS, but takes into account for the possibility of correctly forecasting an event by chance. It varies in the range between -1/3 and 1, being 1 the best value. A value of zero represents a useless forecast, in which the probability of correctly predicting an event is random.

- False Alarm Rate (FAR):

$$FAR = \frac{b}{a+b}$$

which is the ratio between false alarms and number of predicted events and can assume values between 0 and 1. In this case the best value possible is 0. Scores were computed after summing contingency table elements for each model over all simulations (4x30=120 times in this paper, both for the 0-3h and 3-6h forecast interval).

https://doi.org/10.5194/nhess-2023-18
Preprint. Discussion started: 22 February 2023

Natural Hazards and Earth System Sciences
Discussions

Appendix B: The resampling method

The resampling method from Hamill (1999) is used for assessing if score differences are statistically significant in a confidence interval. For this purpose, an hypothesis test is performed. The null hypothesis is that the scores of the considered models do not differ.

In our case, the null hypothesis is that the differences between the two model scores, i.e. BCKG and GPS, are zero. Let S_1 and S_2 be a generic score, namely FBIAS, ETS, POD and FAR (see Appendix 1 for details), for the two model types, BCKG and GPS, respectively. The null hypothesis can be then written as:

$$H_0: S_1 - S_2 = 0$$

The test statistic is calculated after summing contingency table elements for each model over all simulations (4x30=120 times in this paper, both for the 0-3h and 3-6h forecast intervals). The contingency tables can be written as a vector:

$$x_{i,j} = (a, b, c, d)_{i,j}$$

Where *i* is the model type (BCKG or GPS) and *j*=1, …,120 is the contingency table for each time interval.

The contingency table elements are then summed over all times for both model forecasts BCKG and GPS:

$$S_i = f\left(\sum_{j=1}^{n} x_{i,j}\right)$$

and the test statistic is given by the difference between S1 and S2.

Resampled sums can be done after randomly choosing either one or the other model for each time. Let I_j be a random number which can assume values 1 or 2 for BCKG and GPS, respectively, with *j*=1,…,120. We can then sum the shuffled vectors over all times:

$$S_1^* = f\left(\sum_{j=1}^{n} x_{Ij,j}\right)$$

and sum separately data not selected for the first sum, given by the index $(3 - I_j)$:

$$S_2^* = f\left(\sum_{j=1}^{n} x_{(3-Ij),j}\right).$$

Each sample is produced to be consistent with a null distribution, i.e. score differences $(S_1^* - S_2^*)$ are zero.

This random sampling is performed many times (10 000).

We consider the significance levels of α= 0.01, α= 0.05 and α= 0.1 and we test the null hypothesis H_0 with the percentiles. Let $t_L = \frac{\alpha}{2}$ and $t_U = \frac{(1-\alpha)}{2}$.

The null hypothesis H_0 is rejected at the level 90 % (α=0.1), 95%(α=0.05) or 99% (α=0.01) if

$$S_1 - S_2 < t_L$$

https://doi.org/10.5194/nhess-2023-18
Preprint. Discussion started: 22 February 2023

or

$$S_1 - S_2 > t_U$$

where S_1 and S_2 are the non-resampled scores.

Competing interests

The contact author has declared that none of the authors has any competing interests.

References

Barker, D.M., Huang, W., Guo, Y.R and Xiao., Q.N.: A Three-Dimensional (3DVAR) Data Assimilation System For Use With MM5: Implementation and Initial Results. Mon. Weather Rev., 132, 897-914, https://doi.org/10.1175/1520-0493(2004)132<0897:ATVDAS>2.0.CO;2, 2004.

Barker, D., Huang, X.-Y., Liu, Z., Auligné, T. , Zhang, X., Rugg, S., Ajjaji, R., Bourgeois, A., Bray, J., Chen, Y., Demirtas, M., Guo, Y.-R., Henderson, T., Huang, W., Lin, H.-C., Michalakes, J., Rizvi, S., and Zhang, X.: The Weather Research and Forecasting Model's Community Variational/Ensemble Data Assimilation System: WRFDA. B. Am. Meteorol. Soc., 93, 831–843, https://doi.org/10.1175/BAMS-D-11-00167.1, 2012.

Benjamin, S. G., Weygandt, S. S., Brown, J. M., Hu, M., Alexander, C. R., Smirnova, T. G., Olson, J. B., James, E. P., Dowell, D. C., Grell, G. A., Lin, H., Peckham, S. E., Smith, T. L., Moninger, W. R., Kenyon, J. S., and Manikin, G. S.: A North American Hourly Assimilation and Model Forecast Cycle: The Rapid Refresh, Mon. Weather Rev., 144, 1669–1694, https://doi.org/10.1175/MWR-D-15-0242.1, 2016.

Bennitt, G. V. and Jupp, A.: Operational Assimilation of GPS Zenith Total Delay Observations into the Met Office Numerical Weather Prediction Models, Mon. Weather Rev., 140, 2706– 2719, https://doi.org/10.1175/MWR-D-11-00156.1, 2012.

Bevis, M., Businger, S., Herring, T.A., Rocken, C., Anthes, R.A. and Ware, R.H.: GPS meteorology: Remote sensing of atmospheric water vapor using the global positioning system. J. Geophys. Res.-Atmos., 97(D14), pp.15787-15801, https://doi.org/10.1029/92JD01517, 1992.

Boniface, K., Ducrocq, V., Jaubert, G., Yan, X., Brousseau, P., Masson, F., Champollion, C., Chéry, J., and Doerflinger, E.: Impact of high-resolution data assimilation of GPS zenith delay on Mediterranean heavy rainfall forecasting, Ann. Geophys., 27, 2739–2753, https://doi.org/10.5194/angeo-27-2739-2009, 2009.

Caldas-Alvarez, A. and Khodayar, S.: Assessing atmospheric moisture effects on heavy precipitation during HyMeX IOP16 using GPS nudging and dynamical downscaling, Nat. Hazards Earth Syst., 20, 2753–2776, https://doi.org/10.5194/nhess-20-2753-2020, 2020.

Davolio, S., Ferretti, R., Baldini, L., Casaioli, M., Cimini, D., Ferrario, M. E., Gentile, S., Loglisci, N., Maiello, I., Manzato, A., Mariani, S., Marsigli, C., Marzano, F. S., Miglietta, M. M., Montani, A., Panegrossi, G., Pasi, F., Pichelli, E., Pucillo, A.,

530 and Zinzi, A.: The role of the Italian scientific community in the first HyMeX SOP: an outstanding multidisciplinary experience, Meteorol. Z., 24, 261–267, https://www.doi.org/ 10.1127/metz/2015/0624, 2015.

Dudhia, J. Numerical study of convection observed during the Winter Monsoon Experiment using a mesoscale two-dimensional model. J. Atmos. Sci., 46, 3077–3107, https://doi.org/10.1175/1520-0469(1989)046<3077:NSOCOD>2.0.CO;2,1989.

535 Faccani, C., Ferretti, R., Pacione, R., Paolucci, T., Vespe, F. and Cucurull, L.: Impact of a high density GPS network on the operational forecast Adv. Geosci. 2 73–9, https://doi.org/10.5194/adgeo-2-73-2005, 2005.

Federico, S., Torcasio, R. C., Puca, S., Vulpiani, G., Comellas Prat, A., Dietrich, S., Avolio, E.: Impact of Radar Reflectivity and Lightning Data Assimilation on the Rainfall Forecast and Predictability of a Summer Convective Thunderstorm in Southern Italy. Atmosphere-Basel, 12, 958. https://doi.org/10.3390/atmos12080958, 2021.

540 Giannaros, C., Kotroni, V., Lagouvardos, K., Giannaros, T.M., Pikridas, C.: Assessing the Impact of GNSS ZTD Data Assimilation into the WRF Modeling System during High-Impact Rainfall Events over Greece. Remote Sens.-Basel, 12, 383. https://doi.org/10.3390/rs12030383, 2020.

Hamill, T.M.: Hypothesis tests for evaluating numerical precipitation forecasts, Weather Forecast., 14, 155-167, https://doi.org/10.1175/1520-0434(1999)014<0155:HTFENP>2.0.CO;2,1999.

545 Herrera, A.M., Suhandri, H.F., Realini, E., Reguzzoni, M. and de Lacy, M.C.J.G.S.: goGPS: open-source MATLAB software. GPS solut., 20(3), pp.595-603, https://doi.org/10.1007/s10291-015-0469-x, 2016.

Huang, X.Y., Xiao, Q., Barker, D.M., Zhang, X., Michalakes, J., Huang, W., Henderson, T., Bray, J., Chen, Y., Ma, Z., Dudhia, J., Guo, Y., Zhang, X., Won, D.J., Lin, H.C. and Kuo, Y.H.: Four-Dimensional Variational Data Assimilation for WRF: Formulation and Preliminary Results. Mon. Weather Rev., 137, 299–314, https://doi.org/10.1175/2008MWR2577.1, 2009.

550 Janjic, Z. I.: The step-mountain eta coordinate model: Further developments of the convection, viscous sublayer, and turbulence closure schemes. Mon. Weather Rev., 122, 927–945, https://doi.org/10.1175/1520-0493(1994)122<0927:TSMECM>2.0.CO;2,1994.

Lagasio, M., Parodi, A., Pulvirenti, L., Meroni, A.N., Boni, G., Pierdicca, N., Marzano, F.S., Luini, L., Venuti, G., Realini, E., Gatti, A., Tagliaferro, G., Barindelli, S., Monti Guarnieri, A., Goga, K., Terzo, O., Rucci, A., Passera, E., Kranzlmueller, D.,

555 Rommen, B.: A Synergistic Use of a High-Resolution Numerical Weather Prediction Model and High-Resolution Earth Observation Products to Improve Precipitation Forecast. Remote Sens.-Basel, 11, 2387. https://doi.org/10.3390/rs11202387, 2019.

Lindskog, M., Ridal, M., Thorsteinsson, S., Ning, T.: Data assimilation of GNSS zenith total delays from a Nordic processing centre, Atmos. Chem. Phys., 17, 13983–13998, https://doi.org/10.5194/acp-17-13983-2017, 2017.

560 Mascitelli, A., Federico, S., Fortunato, M., Avolio, E., Torcasio, R. C., Realini, E., Mazzoni, A., Transerici, C., Crespi, M., Dietrich, S.: Data assimilation of GNSS-ZTD into the RAMS model through 3D-Var: preliminary results at the regional scale. Meas. Sci. Technol. 30, 055801 (14pp). https://doi.org/10.1088/1361-6501/ab0b87, 2019.

Mascitelli, A., Federico, S., Torcasio, R. C., Dietrich, S.: Assimilation of GPS Zenith Total Delay estimates in RAMS NWP model: Impact studies over central Italy. Adv. Space Res., https://doi.org/10.1016/j.asr.2020.08.031, 68, 12, pp 4783-4793, 2021.

Masson-Delmotte, V., Zhai, P., Pirani, A., Connors, S.L., Péan, C., Berger, S., Caud, N., Chen, Y., Goldfarb, L., Gomis, M.I., Huang, M., Leitzell, K., Lonnoy, E., Matthews, J.B.R., Maycock, T.K., Waterfield, T., Yelekçi, O., Yu, R. and Zhou B.: IPCC, 2021: Climate Change 2021: The Physical Science Basis. In Contribution of Working Group I to the Sixth Assessment 432 Report of the Intergovernmental Panel on Climate Change; Cambridge University Press, 2021.

Mlawer, E.J., Taubman, S.J., Brown, P.D., Iacono, M.J., Clough, S.A.: Radiative transfer for inhomogeneous atmospheres: RRTM, a validated correlated-k model for the longwave. J. Geophys. Res.-Space, 102, 16663–16682, https://doi.org/10.1029/97JD00237, 1997.

Parrish, D.F.; Derber, J.C. The National Meteorological Center's Spectral Statistical Interpolation analysis system. Mon. Weather Rev., 120, 1747–1763, https://doi.org/10.1175/1520-0493(1992)120<1747:TNMCSS>2.0.CO;2, 1992.

Poli, P., Moll, P., Rabier, F., Desrozier, G., Chapnik, B., Berre, L., Healy, S. B., Andersson, E., and El Guelai, F. Z.: Forecast impact studies of zenith total delay data from European near real-time GPS stations in Météo France 4DVAR, J. Geophys. Res.-Atmos., 112, 1–16, https://doi.org/10.1029/2006JD007430, 2007.

Risanto, C.B., Castro, C.L., Arellano Jr, A.F., Moker Jr, J.M., Adams, D.K.: The impact of assimilating GPS precipitable water vapor in convective-permitting WRF-ARW on North American Monsoon precipitation forecasts over Northwest Mexico. Mon. Weather Rev. 149, 3013–3035, https://doi.org/10.1175/MWR-D-20-0394.1,2021.

Roebber, P. J.: Visualizing multiple measures of forecast quality, Weather Forecast., 24, 601–608, https://doi.org/10.1175/2008WAF2222159.1,2009.

Rohm, W., Guzikowski, J., Wilgan, K., and Kryza, M.: 4DVAR assimilation of GNSS zenith path delays and precipitable water into a numerical weather prediction model WRF, Atmos. Meas. Tech., 12, 345–361, https://doi.org/10.5194/amt-12-345-2019, 2019.

Rueger, J.: Refractive indices of light, infrared and radio waves in the atmosphere, U. of New South Wales, Sydney, NSW, Unisurv S-68, 104 pp., 2002.

Saastamoinen, J.: Contributions to the theory of atmospheric refraction, B. Geod., https://doi.org/10.1007/BF02521844, 1972.

Singh, R., Ojha, S.P., Puviarasan, N., Singh, V.: Impact of GNSS signal delay assimilation on short range weather forecasts over the Indian region. J. Geophys. Res.-Atmos., 124, 9855–9873, https://doi.org/10.1029/2019JD030866, 2019.

Skamarock, W.C., Klemp, J.B., Dudhia, J., Gill, D.O., Liu, Z., Berner, J., Wang, W., Powers, J.G., Duda, M.G., Barker, D.M., Huang, X.-Y.: A Description of the Advanced Research WRF Version 4; No. NCAR/TN-556+STR, NCAR Technical Note; National Center for Atmospheric Research: Boulder, CO, USA, 145p, http://dx.doi.org/10.5065/1dfh-6p97, 2019.

Stensrud, D.J., Xue, M., Wicker, L.J., Kelleher, K.E., Foster, M.P., Schaefer, J.T., Schneider, R.S., Benjamin, S.G., Weygandt, S.S., Ferree, J.T., and Tuell, J.P.: Convective-scale Warn-On-Forecast system: A vision for 2020. B. Am. Meteorol. Soc., 90, 1487–1499, https://doi.org/10.1175/2009BAMS2795.1, 2009.

https://doi.org/10.5194/nhess-2023-18
Preprint. Discussion started: 22 February 2023

Trzcina, E., Hanna, N., Kryza, M., Rohm, W.: TOMOREF operator for assimilation of GNSS tomography wet refractivity fields in WRF DA system. J. Geophys. Res.-Atmos., 125, e2020JD032451. https://doi.org/10.1029/2020JD032451, 2020.

Thompson, G.; Field, P.R.; Rasmussen, R.M.; Hall, W.D. Explicit Forecasts of Winter Precipitation Using an Improved Bulk Microphysics Scheme. Part II: Implementation of a New Snow Parameterization. Mon. Weather Rev. 2008, 136, 5095–5115, https://doi.org/10.1175/2008MWR2387.1, 2008.

Vedel, H. and Huang, X.-Y.: Impact of Ground Based GPS Data on Numerical Weather Prediction, J. Meteorol. Soc. Jpn., 82, 459–472, https://doi.org/10.2151/jmsj.2004.459, 2004.

Yan X., Ducrocq V., Poli P., Hakam M., Jaubert G. and Walpersdorf A.: Impact of GPS Zenith delay assimilation on convective-scale prediction of Mediterranean heavy rainfall J. Geophys. Res.-Atmos., 114 D03104, https://www.doi.org/10.1029/2008JD011036, 2009.

Yang, S.-C., Huang, Z.-M., Huang, C.-Y., Tsai, C.-C., Yeh, T.-K.: A case study on the impact of ensemble data assimilation with GNSS-zenith total delay and radar data on heavy rainfall prediction. Mon. Weather Rev. 148, 1075–1098, https://doi.org/10.1175/MWR-D-18-0418.1, 2020.

Zumberge, J.F., Heflin, M.B., Jefferson, D.C., Watkins, M.M. and Webb, F.H.: Precise point positioning for the efficient and robust analysis of GPS data from large networks. J. Geophys. Res.-sol. ea., 102(B3), pp.5005-5017, https://doi.org/10.1029/96JB03860, 1997.